ELSEVIER

Preparing, manipulating, and measuring quantum states on a chip

J.R. Petta[a],*, A.C. Johnson[a], J.M. Taylor[a], E.A. Laird[a], A. Yacoby[b], M.D. Lukin[a], C.M. Marcus[a], M.P. Hanson[c], A.C. Gossard[c]

[a]*Department of Physics, Harvard University, Cambridge, MA 02138, USA*
[b]*Department of Condensed Matter Physics, Weizmann Institute of Science, Rehovot 76100, Israel*
[c]*Materials Department, University of California, Santa Barbara, CA 93106, USA*

Available online 3 November 2006

Abstract

We use gate voltage control of the exchange interaction to prepare, manipulate, and measure two-electron spin states in a GaAs double quantum dot. By placing two electrons in a single dot at low temperatures we prepare the system in a spin singlet state. The spin singlet is spatially separated by transferring an electron to an adjacent dot. The spatially separated spin singlet state dephases in ~ 10 ns due to the contact hyperfine interaction with the GaAs host nuclei. To combat the hyperfine dephasing, we develop quantum control techniques based on fast electrical control of the exchange interaction. We demonstrate coherent spin-state rotations in a singlet–triplet qubit and harness the coherent rotations to implement a singlet–triplet spin echo refocusing pulse sequence. The singlet–triplet spin echo extends the spin coherence time to $1.2\,\mu s$.

1. Introduction

The ability to prepare, manipulate, and measure quantum mechanical coherence has traditionally been confined to the fields of atomic, molecular, and optical physics [1,2]. Recent advances in experimental condensed matter physics have made it possible to demonstrate comparable quantum control in artificially structured solid state systems [3–5]. In this paper we demonstrate how GaAs double quantum dots can be used to prepare, manipulate, and measure quantum states based on the spin degree of freedom of two electrons [6]. These devices form an elementary quantum bit. At the same time, they are a sensitive probe of the environment and can be used to study the basic physics that leads to spin relaxation and spin dephasing [6,7].

Gate defined GaAs/AlGaAs nanostructures have been one of the workhorses of mesoscopic physics [8,9]. It has

recently become possible to isolate a single electron in a gate defined GaAs quantum dot [10]. This work was quickly extended to include more complicated double and triple quantum dots [11–13]. In these systems, electrons can be moved from one quantum dot to another simply by adjusting electrostatic potentials using DC gate voltages. Manipulating these gate voltages using high-speed techniques has enabled coherent manipulation of the charge degree of freedom [14]. In this paper, we will describe how fast gate voltage control can be used to manipulate two-electron spins that are coupled together by a tunable exchange interaction [6,7,15].

2. Experimental details

Gate defined double quantum dots are fabricated from a GaAs/Al$_{0.3}$Ga$_{0.7}$As heterostructure grown by molecular beam epitaxy (Fig. 1). The two-dimensional electron gas (2DEG) has an electron density of $2 \times 10^{11}\,cm^{-2}$ and a mobility of $2 \times 10^{5}\,cm^{2}/V\,s$. Electrical contact to the 2DEG is made by depositing AuGe wirebonding pads,

*Corresponding author. Tel.: +609 258 1173.
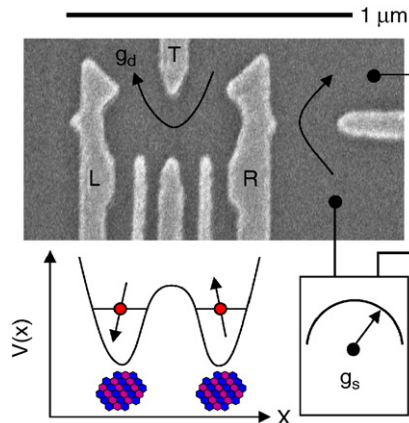*E-mail address:* petta@princeton.edu (J.R. Petta).

Fig. 1. Scanning electron microscope (SEM) image of a few-electron double quantum dot. The double dot may be probed by measuring the double dot conductance, g_d, or by measuring the quantum point contact charge sensor conductance, g_s. When the gates are appropriately biased, a double well potential is formed. Gates L(R) primarily tune the number of electrons in the left(right) dot. Gate T is used to tune the interdot tunnel coupling. The lattice nuclei couple to the electron spins through the contact hyperfine interaction.

which are then annealed using a rapid thermal annealer. Gate electrodes are patterned using standard electron beam lithography and liftoff techniques. By applying negative voltages to the gates, we create a double well potential. The number of electrons in the left and right dots are tuned primarily by adjusting $V_L(V_R)$, while the barrier separating the two dots is adjusted using V_T. Conductance through the double dot, g_d, and the quantum point contact conductance, g_s, are measured using standard lock-in techniques.

Measurements are performed in a dilution refrigerator with a base temperature of 40 mK. The electron temperature is $T_e \sim 135$ mK, as determined from Coulomb blockade peak widths. To manipulate the double quantum dot on nanosecond timescales we apply pulses to the gates L and R using a Tektronix AWG520 pulse generator. Pulses are transmitted to the sample using semi-rigid coax cables, which are thermally anchored and electrically filtered using SMA attenuators. Pulse signals and DC voltages are combined at the mixing chamber using Anritsu bias tees [16].

Quantum dots are typically probed by measuring the conductance through the dot. Coulomb blockade peaks are measured as a gate voltage tunes the electrostatic energy of the dot. For a double quantum dot the device behavior is slightly more complicated [17]. Since the device consists of two quantum dots connected in series, it is only possible to measure a resonant tunneling current when both the left and right dots are tuned to a Coulomb blockade resonance. In addition, since the right and left dot are coupled together capacitively, the electrostatic energy of the right dot is sensitive to the number of electrons in the left dot (and vice versa).

Transport measurements of the double dot conductance can be used to characterize the device and tune the tunnel
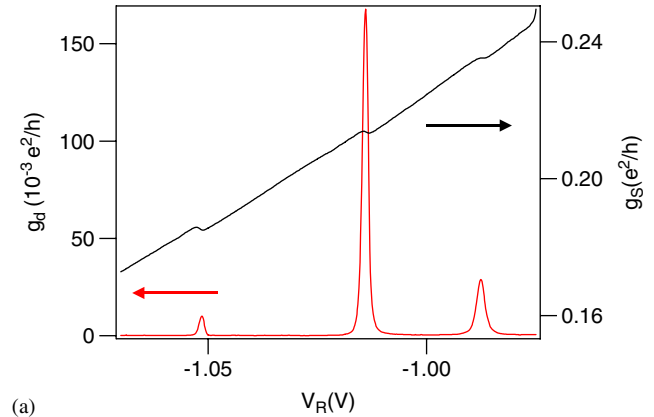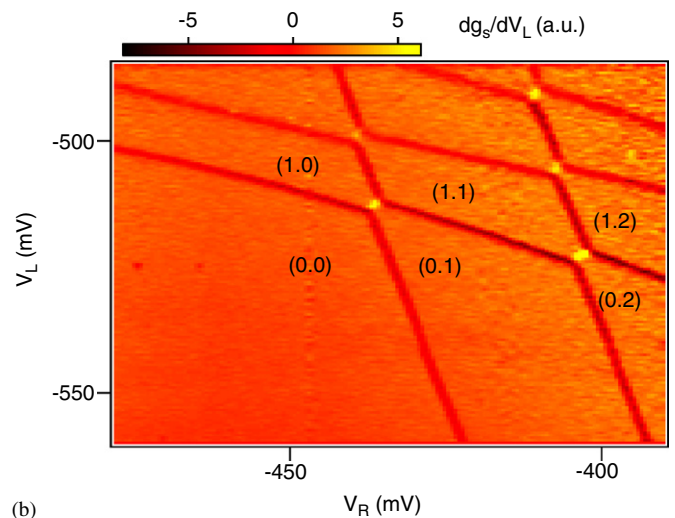
Fig. 2. Transport and charge sensing measurements of the double dot. (a) Simultaneous measurement of g_d and g_s as a function of V_R. The double dot is tuned to large interdot tunnel coupling so that the device behaves similar to a single quantum dot. Increasing V_R adds electrons to the double dot, resulting in Coulomb blockade peaks in g_d. Direct capacitive coupling between V_R and the QPC results in an increase in g_s with V_R. In addition to this simple cross-coupling, each time an electron is added to the dot, g_s decreases. (b) Charge stability diagram obtained by measuring dg_s/dV_L as a function of V_L and V_R. In the lower left corner of this image, the double dot is empty, denoted $(0, 0)$.

rates. However, to create a quantum bit with a long coherence time it is not advantageous to continuously probe the system by sending electrons through the double quantum dot. In addition, it is not always possible to reliably determine the absolute number of electrons in the double quantum dot since the tunnel coupling to the leads can be too small to measure transport while the quantum dot still contains electrons. For these reasons, we will in the remainder of the paper focus on measurements obtained using a quantum point contact charge sensor [11,18,19].

Fig. 2(a) shows measurements of the double dot conductance and the quantum point contact charge sensor conductance as a function of gate voltage in the limit of large interdot tunnel coupling (where the device behaves similar to a single quantum dot). As the gate voltage is swept, Coulomb blockade peaks are observed in g_d. For increasing V_R, the QPC conductance increases due to

direct capacitive coupling between the gate and the quantum point contact. In addition, each time an electron is added to the double dot by sweeping the gates through a Coulomb blockade peak, the QPC conductance decreases by a small amount. Adding an electron to the double dot effectively reduces the QPC channel width. These data show that the QPC is sensitive to the electrostatic configuration of the double dot, as first demonstrated in single dots by Field et al. [18].

The full charge stability diagram for this device is determined by measuring the QPC conductance as a function of V_L and V_R. This is then numerically differentiated with respect to V_L. A resulting plot of dg_s/dV_L as a function of V_L and V_R is shown in Fig. 2(b). In the lower left corner of this plot, the double dot is completely depleted and no charge transitions are observed. We label this as a $(0,0)$ charge state. Increasing V_L adds a single electron to the left dot, creating a $(1,0)$ charge state. By navigating in this charge stability diagram using the DC gate voltages, the occupancy of the double dot can be easily tuned.

3. Singlet–triplet spin qubit

We have demonstrated control of a spin qubit based on two-electron spin states [6]. This qubit was first proposed by Levy et al. and has the advantage that the qubit is insensitive to overall magnetic field fluctuations [20]. In addition, the qubit can be controlled using electrical techniques and magnetic field gradients [21]. Here we describe the physics behind qubit operation.

The singlet–triplet qubit operates in the two-electron regime. We work such that there are either two electrons in the right dot, denoted $(0,2)$, or such that there is one electron in each dot, denoted $(1,1)$. In the $(0,2)$ charge state, tight confinement of the electrons leads to a large singlet–triplet splitting, $J \sim 0.5$ meV. We will take advantage of this large singlet–triplet splitting to initialize the spin qubit and to perform spin-to-charge conversion to read out the state of the spin qubit. The singlet–triplet splitting of the $(1,1)$ charge state is set by the interdot tunnel coupling and scales as $j \sim 4t^2/U$. For realistic interdot tunnel couplings, $t \sim 4$ GHz ~ 16 µeV and charging energies $U \sim 3$ meV, $j < 1$ µeV and the singlet and triplet states are nearly degenerate. By transferring an electron from the $(0,2)$ charge state to the $(1,1)$ charge state, the singlet–triplet splitting can be tuned. The full energy-level diagram is illustrated in Fig. 3(a).

3.1. Qubit initialization

Fig. 4 shows the charge stability diagram in the two-electron regime as determined using the quantum point contact charge detector. g_s measured as a function of V_L and V_R shows four distinct levels, corresponding to the charge states $(0,1)$, $(1,1)$, $(0,2)$, and $(1,2)$. As electrons are added to the double dot, g_s decreases, as expected. To
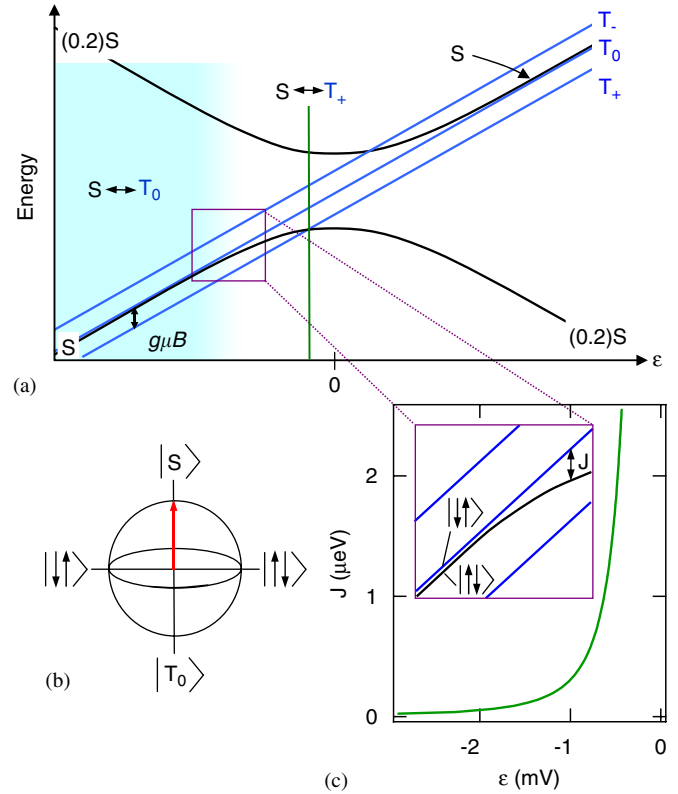

Fig. 3. (a) Energy-level diagram for the singlet–triplet qubit. At positive detunings, the ground state is $(0,2)S$. For negative detunings, and at finite fields, $|S\rangle$ and $|T_0\rangle$ are nearly degenerate. At zero field, the triplet states are degenerate. (b) Bloch sphere representation of the singlet–triplet qubit. (c) Hybridization of the $(1,1)$ and $(0,2)$ charge states results in an exchange splitting, $J(\varepsilon)$, which is a sensitive function of detuning.
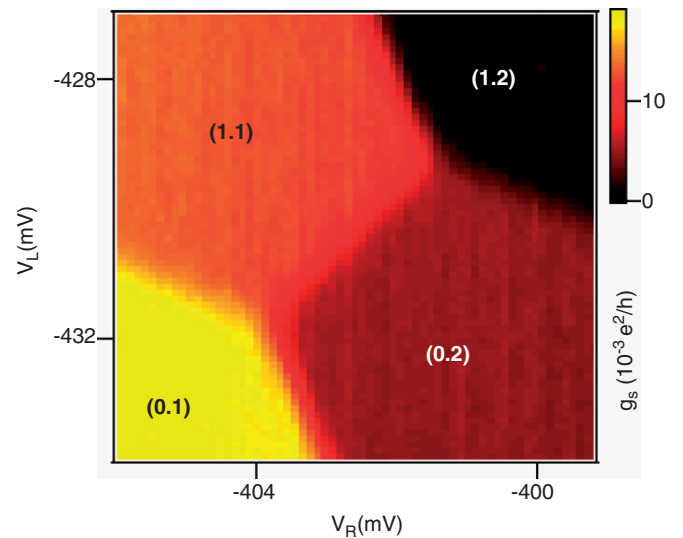

Fig. 4. Charge stability diagram in the two-electron regime obtained by measuring g_s as a function of V_L and V_R.

initialize the qubit, the gate voltages are set such that the Fermi level of the leads lies in-between the $(0,2)$ singlet and triplet spin states. A high-energy spin triplet state will relax to a spin singlet state through a process in which an electron is exchanged with the Fermi sea.

3.2. Qubit manipulation

Manipulation of the quantum bit takes place using pulsed gate techniques [15,22]. As described above, the exchange energy can be tuned by setting the detuning. At positive detunings, the double dot is in the $(0, 2)$ charge state and the singlet–triplet splitting is $\sim 0.5\,\mathrm{meV}$. For negative detunings, the electrons are separated in the $(1, 1)$ charge state and the singlet–triplet splitting is set by the interdot tunnel coupling. Near the interdot charge transition, the singlet–triplet splitting, $J(\varepsilon)$, is very sensitive to the detuning.

To understand the role of the exchange energy, we draw the states of the spin qubit using the Bloch sphere representation shown in Fig. 3(b). $|S\rangle$ is located at the north pole of the Bloch sphere and $|T_0\rangle$ at the south pole. Product states $|\uparrow\downarrow\rangle$ and $|\downarrow\uparrow\rangle$ are located on the $\pm x$-axis directions. If we initialize the spin qubit into the product state $|\uparrow\downarrow\rangle$, turning on the exchange will drive a rotation in this Bloch sphere representation by an angle $\phi = J(\varepsilon)\tau/\hbar$ about the z-axis. An appropriately timed pulse will rotate $|\uparrow\downarrow\rangle$ to $|\downarrow\uparrow\rangle$, which is called a SWAP operation. Exchange driven rotations will be demonstrated below. Field gradients, due to external fields or internal variations in the nuclear spin configuration, drive x-axis rotations in this representation.

3.3. Qubit read-out

We use spin-to-charge conversion to read-out the spin state of the qubit. In the two electron system, Pauli exclusion leads to rectification in DC transport [7,23,24]. A $(1, 1)$ triplet to $(0, 2)$ singlet transition is blocked. We utilize these spin-dependent transitions to determine the spin state of the qubit. In general, the qubit is manipulated in the $(1, 1)$ charge state. After manipulation, we read-out the spin state by applying a pulse to the gates, which tilts the double well potential so that the $(0, 2)$ singlet state is the ground state. A $(1, 1)$ singlet state will tunnel directly to $(0, 2)$ singlet. However, a $(1, 1)$ triplet state cannot tunnel to $(0, 2)$ singlet due to the spin blockade. Since the triplet remains in $(1, 1)$ and the singlet tunnels to $(0, 2)$, a charge sensor can be used to determine the spin state.

4. Relaxation, dephasing, and quantum control

We now combine state preparation, manipulation, and read-out to measure the spin relaxation and dephasing times in the two-electron system. We then demonstrate coherent control.

4.1. Spin relaxation

Several groups have measured spin relaxation times in single quantum dots using electrical and optical techniques [22,25–27]. There are many theoretical calculations of spin relaxation times for quantum dots [28–32]. Spin relaxation times in the singlet–triplet qubit were measured by Johnson et al. [7]. To measure the spin relaxation time, we operate the device as a charge pump. Fast gate voltage control is used to drive charge transitions from $(0, 1)$ to $(1, 1)$ to $(0, 2)$. This control sequence corresponds to pulsing the gates around a triple point in the charge stability diagram.

In the first step of the pulse sequence, an electron is added to the double dot to create a $(1, 1)$ charge state. Either a singlet or one of the three triplet states is created since the $(1, 1)$ singlet and triplet states are nearly degenerate. Due to the three-fold degeneracy of the triplet states, we create a $(1, 1)$ triplet state on average 75% of the time. To measure the decay time of a triplet state to the $(0, 2)$ singlet state, we apply a second pulse which tilts the double well potential such that the $(0, 2)$ singlet state is the ground state. The $(1, 1)$ triplet to $(0, 2)$ singlet transition is blocked due to the spin blockade. After a T_1 time, the triplet state will relax to the $(1, 1)$ singlet state, which is followed by a transition to $(0, 2)$ singlet. This transition is registered by the charge sensor. Finally, a third pulse is applied to the sample which ejects an electron from the double dot, leaving it in a $(0,1)$ charge state. This pulse sequence is repeated continuously while g_s is measured as a function of the DC gate voltages.

Experiments measured the decay time as a function of field and detuning. For $B = 150\,\mathrm{mT}$, decay times exceeding 1 ms were measured. However, at low magnetic fields, the decay time was much faster and the triplet states relaxed on microsecond timescales. A simple model taking into account the hyperfine interaction with the nuclear spins captures the observed field and detuning dependence. We refer the reader to Ref. [7] for details of the experiment and theory.

4.2. Spin dephasing

Due to the contact hyperfine interaction with the lattice nuclei, two spatially separated electron spins will experience distinct hyperfine fields. In a semi-classical picture, they will precess around these effective fields at different rates, which leads to a spin state rotation in the $|S\rangle$, $|T_0\rangle$ basis. To measure the spin dephasing time, we first initialize the qubit at positive detuning where the ground state is $(0, 2)S$. The spin singlet is then spatially separated by decreasing detuning slowly with respect to the tunnel coupling. Once separated, the electrons evolve in the presence of the hyperfine fields. To measure the amount of dephasing that takes place during the separation time, τ_S, we perform spin to charge conversion. The detuning is increased to make $(0, 2)S$ the ground state. If the separated spins remain in the singlet state, $|S\rangle$ will adiabatically follow to $(0, 2)S$. However, if the separated spins mixed into a triplet state, the charge transition to $(0, 2)S$ will be blocked due to Pauli exclusion. The quantum point contact can then be used to read-out the spin state.
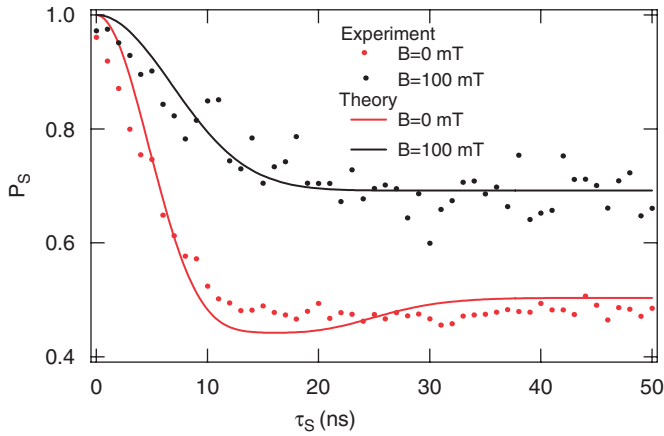
Fig. 5. Singlet state probability, P_S, measured as a function of separation time, τ_S. Data points are acquired at $B = 0$ and 100 mT. Solid lines are best fits to the data using a semi-classical model of the hyperfine interaction.

Fig. 5 shows the singlet state probability, P_S, measured as a function of the separation time, τ_S. Data are collected at $B = 0$ and 100 mT. P_S decays on a 10–20 ns timescale and saturates at long time values of 0.5 (0.7) for $B = 0$ ($B = 100$ mT). The singlet state decay is Gaussian and can be fit using a simple semi-classical model [33,34]. A best fit decay time results in $T_2^* \sim 10$ ns, which corresponds to a hyperfine field $B_{nuc} \sim 2.3$ mT. Differences in the long time value of τ_S are due to the spin state degeneracy. At zero field, $|S\rangle$ can rotate into all three triplet states. For $B \gg B_{nuc}$, the $|T_+\rangle$ and $|T_-\rangle$ triplet states are split off by the Zeeman energy and $|S\rangle$ can only mix into the $|T_0\rangle$ state. A second fit parameter accounts for the efficiency of the spin state read-out.

4.3. Quantum control

The measurement above shows that two spatially separated electron spins will dephase in ~ 10 ns due to the contact hyperfine interaction with the GaAs lattice nuclei. To combat this hyperfine dephasing, we have developed quantum control techniques based on fast electrical control of the exchange interaction. This control allows us to drive coherent spin state rotations as well as implement a singlet–triplet spin echo refocusing pulse sequence. As illustrated above, the hyperfine fields lead to fast spin dephasing. However, there is a large separation of time-scales in the system and the electron spin dynamics occur on a much shorter timescale than the nuclear spin dynamics. For this reason, a spin echo pulse sequence is very efficient at refocusing the spin singlet state.

To demonstrate coherent control, we first prepare the system in a spin singlet state, $(0, 2)S$. The singlet state is then spatially separated by decreasing detuning slowly with respect to the hyperfine mixing rate. With $J \sim 0$, the separated electrons load into the ground state of the hyperfine fields. We define this as an $|\uparrow\downarrow\rangle$ spin state, which

is located on the x-axis of the Bloch sphere. Coherent rotations are achieved by turning on the exchange interaction for a time τ_E by increasing the detuning. This results in a rotation of the spin state by an angle $\phi = J(\varepsilon)\tau_E/\hbar$ about the z-axis of the Bloch sphere. After this rotation, the resulting spin state is measured by increasing the detuning and projecting back onto the $|S\rangle$, $|T_0\rangle$ states. Fig. 6 shows coherent oscillations in P_S measured using this pulse sequence. By increasing the tunnel coupling, which in turn increases the exchange energy, we can achieve a $\sqrt{\text{SWAP}}$ in ~ 180 ps.

These coherent rotations can be harnessed to implement a "singlet–triplet spin echo" pulse sequence. In the presence of the hyperfine fields, the spatially separated singlet state $|S\rangle$, will rotate around the x-axis of the Bloch sphere into the state $|T_0\rangle$. The rotation rate depends on the field difference between the left and right dots. Since the hyperfine fields vary on a ~ 100 μs timescale, this rotation rate varies from run to run and is uncontrolled.

The random hyperfine rotation can be corrected for by implementing a spin echo pulse sequence. A singlet state is prepared. In the Bloch sphere picture, the Bloch vector points at the north pole of the Bloch sphere. Once the
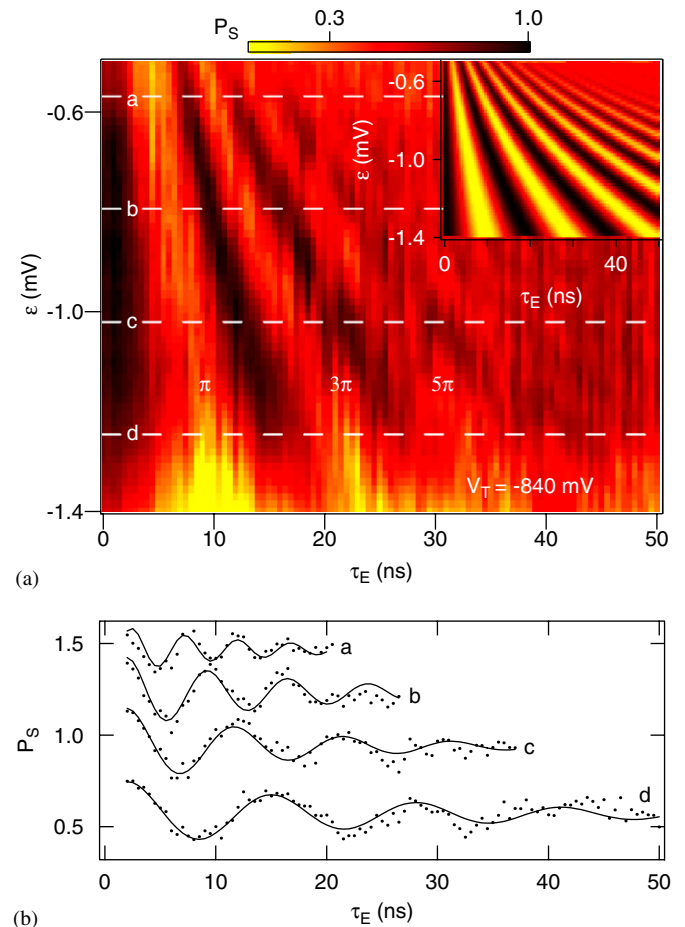

Fig. 6. Exchange driven spin state rotations. (a) P_S shows oscillations as a function of the exchange pulse time, τ_E, and as a function of ε. (b) Horizontal cuts through the data in (a).
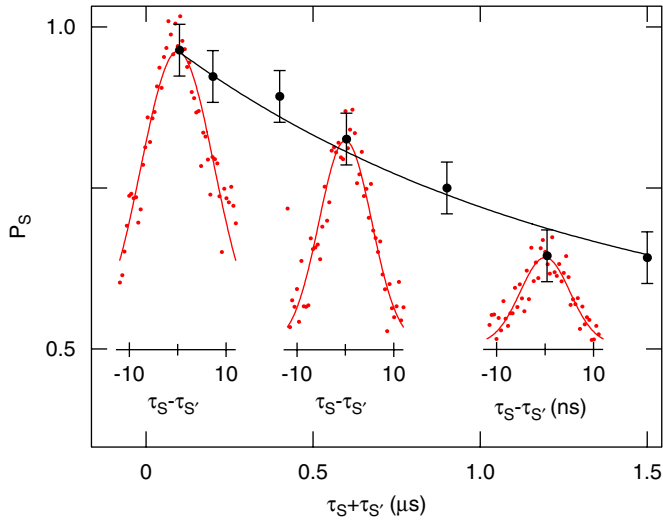
Fig. 7. Spin echo refocusing. Measurements of the singlet state probability, P_S as a function of $\tau_S-\tau_{S'}$ for several values of the total separation time $\tau_{tot} = \tau_S + \tau_{S'}$. A best fit to the data gives $T_2 = 1.2\,\mu s$. We have been able to extend this time by increasing the magnetic field and using higher-order correction pulse sequences (Carr–Purcell).

electrons are separated, the hyperfine fields drive a rotation between $|S\rangle$ and $|T_0\rangle$. After some separation time, τ_S, we perform a π pulse about the z-axis of the Bloch sphere by turning on the exchange. Exchange is then turned off, and the system evolves in the hyperfine fields for a time $\tau_{S'}$. During this time, the hyperfine fields rotate the Bloch vector back toward the north pole of the Bloch sphere. If $\tau_{S'} = \tau_S$, and the hyperfine fields do not vary during the pulse sequence, refocusing occurs, and the spin singlet state is recovered. Fig. 7 shows P_S measured as a function of $\tau_S-\tau_{S'}$, for several values of the total separation time $\tau_{tot} = \tau_S + \tau_{S'}$. The spin echo preserves the spin singlet state for times exceeding $1.2\,\mu s$.

5. Conclusions

We have demonstrated that a double quantum dot can be used to create a singlet–triplet spin qubit. The spin qubit has a long lifetime, $T_1 \sim 10\,ms$. We showed that two spatially separated spins dephase in $\sim 10\,ns$ due to the contact hyperfine interaction with the GaAs host nuclei. Fast control of the exchange interaction can be used to drive coherent rotations and to implement a singlet–triplet spin echo pulse sequence. Using these quantum control

techniques, we have been able to demonstrate a coherence time T_2, exceeding $1.2\,\mu s$.

References

[1] M. Brune, et al., Phys. Rev. Lett. 76 (1996) 1800.
[2] C.J. Hood, et al., Phys. Rev. Lett. 80 (1998) 4157.
[3] Y. Nakamura, et al., Nature 398 (1999) 786.
[4] A. Wallraff, et al., Nature 431 (2004) 162.
[5] J.M. Martinis, et al., Phys. Rev. Lett. 89 (2002) 117901.
[6] J.R. Petta, et al., Science 309 (2005) 2180.
[7] A.C. Johnson, et al., Nature 435 (2005) 925.
[8] B.J. VanWees, et al., Phys. Rev. Lett. 60 (1988) 848.
[9] J.A. Folk, et al., Phys. Rev. Lett. 76 (1996) 1699.
[10] M. Ciorga, et al., Phys. Rev. B 61 (2000) 16315.
[11] J.M. Elzerman, et al., Phys. Rev. B 67 (2003) 161308.
[12] J.R. Petta, et al., Phys. Rev. Lett. 93 (2004) 186802.
[13] L. Gaudreau, et al., Phys. Rev. Lett. 97 (2006) 036807.
[14] T. Hayashi, et al., Phys. Rev. Lett. 91 (2003) 226804.
[15] J.R. Petta, et al., Phys. Rev. B 72 (2005) R161301.
[16] Anritsu Company, Model K251.
[17] W.G. van der Wiel, et al., Rev. Mod. Phys. 75 (2003) 11.
[18] M. Field, et al., Phys. Rev. Lett. 70 (1993) 1311.
[19] L. DiCarlo, et al., Phys. Rev. Lett. 92 (2004) 226801.
[20] J. Levy, et al., Phys. Rev. Lett. 89 (2002) 147902.
[21] J.M. Taylor, et al., Nature Phys. 1 (2005) 177.
[22] T. Fujisawa, et al., Nature 419 (2002) 278.
[23] K. Ono, et al., Science 297 (2002) 1313.
[24] F.H.L. Koppens, et al., Science 309 (2005) 1346.
[25] R. Hanson, et al., Phys. Rev. Lett. 91 (2003) 196802.
[26] J.M. Elzerman, et al., Nature 430 (2004) 431.
[27] M. Kroutvar, et al., Nature 432 (2004) 81.
[28] A.V. Khaetskii, Y.V. Nazarov, Phys. Rev. B 61 (2000) 12639.
[29] S.I. Erlingsson, Y.V. Nazarov, V.I. Fal'ko, Phys. Rev. B 64 (2001) 195306.
[30] A.V. Khaetskii, D. Loss, L. Glazman, Phys. Rev. Lett. 88 (2002) 186802.
[31] I.A. Merkulov, Al.L. Efros, M. Rosen, Phys. Rev. B 65 (2002) 205309.
[32] V.N. Golovach, A. Khaetskii, D. Loss, Phys. Rev. Lett. 93 (2004) 016601.
[33] K. Schulten, P.G. Wolynes, J. Chem. Phys. 68 (1978) 3292.
[34] J.M. Taylor et al., cond-mat/0602470.